Unambiguous Doppler Shift Estimation for Moving Targets with High Range Velocity Using SAR Data*

Paulo A. C. Marques and José M. B. Dias

Abstract

This paper presents a new methodology to retrieve slant-range velocity estimates of moving targets inducing Doppler-shifts beyond the Nyquist limit determined by the pulse repetition frequency (PRF). The proposed approach exploits the linear dependence (not subject to PRF limitations) of the Doppler-shift with respect to the slant-range velocity, at each wavelength. Basically, we propose an algorithm to compute the skew of the two-dimensional spectral signature of a moving target. Distinctive features of this algorithm are its ability to cope with strong range migration and its efficiency from the computational point of view. By combining the developed scheme to retrieve the slant-range velocity with a methodology proposed elsewhere to estimate the velocity vector magnitude, the full velocity vector is unambiguously retrieved without increasing the mission PRF. The effectiveness of the method is illustrated with simulated and real data. As an example, slant-range velocities of moving objects with velocities between 6 and 12 times the Nyquist velocity are estimated with accuracy better than 3%.

Keywords

Synthetic aperture radar, moving targets, velocity estimation, Doppler-shift ambiguity resolution.

I. Introduction

A moving target induces in the synthetic aperture radar (SAR) returned signal a Doppler-shift and a Doppler-spread in the slow-time[1] frequency domain [2]. Most techniques proposed in the recent literature to image moving targets and estimate their velocity parameters take advantage of this knowledge e.g., [3], [4], [5], [6]. Assuming a broadside geometry, the cross-range and slant-range velocities of a moving target are responsible for the spread and for the Doppler-shift, respectively, both in the slow-time frequency domain. Given a pulse repetition frequency (PRF), the Doppler-shift $f_D = 2v_x/\lambda$, where v_x is the target slant-range velocity and λ is the signal wavelength, is confined to

$$\frac{-PRF}{2} < f_D \leq \frac{PRF}{2}. \tag{1}$$

If the received signal is aliased (i.e., the induced Doppler-shift exceeds $PRF/2$) it has been generally accepted that the true moving target slant-range velocity cannot be uniquely determined using a single antenna and a single pulse scheduling [7], [8]. Classical solutions to process such targets with a single

*This work was supported by the Fundação para a Ciência e Tecnologia, under the project POSI/34071/CPS/2000.

[1]Herein, we follow Soumekh's terminology (see [1, Ch. 2]) according to which the cross-range coordinates and the round-trip time are termed *slow-time* and *fast-time* domain, respectively. This terminology stems from the fact that the motion of the radar platform is much slower than the light speed at which the transmitted and backscattered pulses propagate.

antenna consist in increasing the PRF [7] or, alternatively, in using a non-uniform PRF as proposed in [8] and [9]. Increasing the PRF shortens the unambiguous range swath and increases the memory requirements to store the received signal. The use of a non-uniform PRF requires a non-conventional pulse scheduling. Moreover, non-uniform sampling introduces complexity in image reconstruction algorithms.

The approach herein proposed to estimate the slant-range velocity of moving targets with velocities above the Nyquist limit takes advantage of the linear dependence of the Doppler-shift on the slant-range velocity, at each fast-time frequency. In the two-dimensional frequency domain, a moving target echo exhibits a skew not subject to PRF limitations. In [10] this fact has already been exploited to retrieve the spectral support of SAR signals, with application to low contrast ground scenes in spaceborne SAR. In these scenarios the ground behaves as a moving target due to the earth rotation relatively to the radar platform. The technique proposed therein works by applying a linear regression on the estimated Doppler centroids at each fast-time frequency. The problem that we are dealing with in this work cannot be solved by the same technique, because we are interested in returns from near point-like moving targets (e.g., many man-made objects), relatively to the ground. Even after digitally spotlighting[2] the moving target signatures [1], the ground echoes exhibit sufficient power to corrupt the estimates given by spectral centroid type estimators. In this paper we present a technique able to cope with this scenario. For scenes with high signal to clutter ratio (SCR) the proposed estimator is effective, even when the ground echoes are completely superimposed, in the frequency domain, on the moving objects echoes.

This paper is organized as follows. In section II we review basic properties of moving target echoes in SAR and present the proposed methodology to retrieve unaliased estimates of the slant-range velocity. In section III we show results taking real and simulated data to illustrate the effectiveness of the proposed scheme. In appendix we derive expressions supporting the main text and compute theoretical bounds.

[2] i.e., cropping small areas of focused or roughly focused scenes.

II. Proposed Aproach

In [3], [11] we have shown that the returned echo $A(k_u, k)$ from a moving target takes, in the slow-time frequency domain[3] k_u and fast-time frequency domain $k \equiv 2\pi/\lambda$, the shape of the two-way antenna radiation pattern g according to

$$A(k_u, k) \propto g\left(\frac{1}{2\nu}(k_u - 2k\mu)\right), \tag{2}$$

where $\nu \equiv (1 + v_y/V)$ and $\mu \equiv v_x/V$ denote, respectively, the moving target relative cross-range and slant-range velocities, with respect to the sensor velocity V. Relatively to a static target, the shape g becomes shifted by $2k\mu$ and expanded by 2ν. If the transmitted pulse has bandwidth B, then k is confined to

$$k_{min} \cong -\frac{\pi B}{c} + k_0 < k \leq k_0 + \frac{\pi B}{c} \cong k_{max}, \tag{3}$$

where $k_0 \equiv 2\pi/\lambda_0$, λ_0 is the carrier wavelength, and c is the propagation speed. For a moving target with relative slant-range velocity μ, we see from expression (2) that the support of the returned signal $S(k_u, k)$ exhibits a slope of 2μ with respect to the k axis, as illustrated in Fig. 1. In this figure, $k_{u_{end}}$ and $k_{u_{start}}$ denote the Doppler-shifts at the fast-time frequencies k_{max} and k_{min}, respectively. We conclude then that

$$\mu = \frac{k_{u_{end}} - k_{u_{start}}}{2(k_{max} - k_{min})}, \tag{4}$$

regardless of the PRF. In the absence of electronic noise and ground clutter, $k_{u_{end}}$ and $k_{u_{start}}$ could

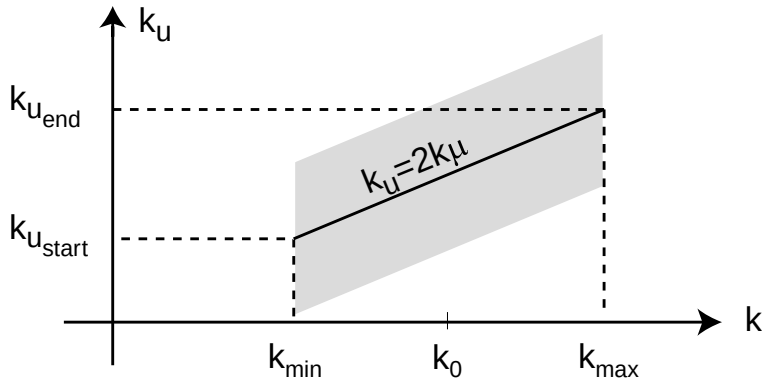

Fig. 1. Domain of the returned signal from a moving target with relative range velocity μ.

be inferred using a simple centroid technique. This solution cannot, however, be applied in the case of ground moving targets, because the returned signal co-exists with clutter returns in the 2D spectrum. The weight of the clutter can be reduced by spotlighting the moving target area, after focusing with approximated moving target parameters (e.g., static ground parameters). However, the spotlighted area cannot be made arbitrary small because moving targets are defocused, for we use approximated

[3]In classical SAR jargon, k_u is termed Doppler domain.

moving target parameters in focusing the SAR image. As an illustration of the spotlight region dimensions see Fig. 8in the Estimation Results section, where the static ground appears focused and two moving vehicles appear strongly blurred, thus occupying a larger area than their actual dimensions.

We show in appendix that if the number of the ground scatterers is large, none is predominant, and they are uniformly distributed within a wavelength, then the correlation of the static ground returns, in the (k_u, k) domain decays very quickly in both dimensions. Concerning moving targets, the same is not true, as it will be seen in the next subsection. Thus, the signal echoed by moving targets have statistical properties quite different from those of the clutter. In this work we will exploit these distinct properties to derive a methodology to unambiguously estimate moving target slant-range velocities.

The received signal from a moving target in the 2D Fourier domain (k_u, k), after pulse compression, is given by [3], [11]

$$S_m(k_u, k) = |P(\omega)|^2 A(k_u, k) f_m e^{-j\sqrt{4k^2 - \left(\frac{k_u}{\alpha}\right)^2}X} e^{-j\frac{k_u}{\alpha}Y}, \tag{5}$$

where $P(\omega)$ is the Fourier transform of the transmitted signal, f_m is the moving target complex reflectivity, (X, Y) are the motion transformed coordinates (see [1, Ch. 6.7] for more details), and $\alpha = \sqrt{\mu^2 + \nu^2}$ is the relative speed of the moving target with respect to the radar.

The correlation function $R_{SS}(\Delta k_u, k_1, k_2)$ between $S_m(k_u, k_1)$ and $S_m(k_u, k_2)$ with respect to k_u is

$$R_{SS}(\Delta k_u, k_1, k_2) = \int_{-\infty}^{+\infty} S_m(k_u, k_1) S_m^*(k_u - \Delta k_u, k_2) dk_u. \tag{6}$$

From (2) we can write $A(k_u, k_1 + \Delta k) = A(k_u - 2\Delta k\mu, k_1)$. Using this fact and after some algebraic manipulation, we are lead to

$$\begin{aligned} &R_{SS}(\Delta k_u, k_1, k_1 + \Delta k) \approx \\ &\quad |P(\omega_1)|^2 |P(\omega_2)|^2 |f_m|^2 e^{-j\left[\frac{\Delta k_u}{\alpha}Y - \left(2\Delta k - \frac{\Delta k_u^2}{4(k_1+\Delta k)\alpha^2}\right)X\right]} \\ &\times \int_{-\infty}^{+\infty} A(k_u, k_1) A^*(k_u - 2\Delta k\mu - \Delta k_u, k_1) e^{j\phi} dk_u, \end{aligned} \tag{7}$$

where $\omega_1 = k_1 c$, $\omega_2 = k_2 c$, $\Delta k = k_2 - k_1$, and

$$\phi = \frac{2k_u \Delta k_u}{4(k_1 + \Delta k)\alpha^2} X. \tag{8}$$

If phase ϕ has an excursion smaller than π in the Doppler interval equivalent to the antenna bandwidth, the last line of (7) is a correlation between $A(k_u, k_1)$ and $A(k_u - 2\Delta k\mu, k_1)$, with respect to k_u, computed at Δk_u. Correlation $R_{SS}(\Delta k_u, k_1, k_1 + \Delta k)$ exhibits a maximum linearly dependent on Δk by a factor of 2μ. The maximum relative slant-range velocity that can be estimated using this methodology is thus imposed by the above referred restriction on phase ϕ. Considering that the maximum magnitude of the correlation R_{SS} occurs at $\Delta k_u = 2\Delta k\mu$, the antenna bandwidth is B_u, and the

relative velocity is $\alpha \approx 1$, then the relative slant-range velocity that can be estimated is bounded by

$$|\mu| < \frac{(k + \Delta k)\pi}{B_u \Delta k X}. \tag{9}$$

Bound (9) can be made larger by compensating in (5) the dependency on X using the target area approximate slant-range coordinates; i.e., multiplying signal $S_m(k_u, k)$ in (5) by $\exp\{j\sqrt{4k^2 - (k_u/\alpha')^2}X'\}$ where X' is the target approximate slant-range coordinate in the unfocused image and $\alpha' \approx 1$. In this way, phase ϕ, although not completely compensated, will exhibit a smaller excursion.

As a numerical example of bound (9), let us consider the AER-II SAR system parameters mentioned in [12] and an error of 50 m in the slant-range coordinate X of the moving target. Assuming the Transall aircraft cruise speed of 495 km/h, the maximum unambiguous velocity is approximately 200km/h, which is sufficient for most man made ground vehicles.

Another possibility to make the limit (9) less tight consists in partitioning the overall pulse-bandwidth into smaller bands, and computing μ by averaging the estimates of all bands.

In deriving (7) we have assumed that the antenna pattern $A(k_u, k)$ does not depend on the wavenumber k in the pulse bandwidth interval. This is valid for planar antennas [1, Ch. 6.3]. In the case of a curved radar aperture the antenna pattern depends on k. Nevertheless, this dependency does not invalidate the concepts just presented as its effect does not occur in the Doppler domain.

A. Proposed methodology

We have just concluded that the maximum magnitude of the correlation between $S_m(k_u, k_1)$ and $S_m(k_u, k_2)$ occurs at $\Delta k_u = 2\Delta k\mu$ (assuming that phase ϕ excursion is smaller than π). This fact could be used to derive a maximum likelihood estimator of μ. However, the signal S_m depends on the unknown parameters $(X, Y, \alpha, A(k_u, k))$, besides the parameter μ in which we are interested. This introduces complexity in the maximum likelihood approach. For this reason we adopt herein a suboptimal solution that is simpler and, nevertheless, effective.

In a realistic SAR scenario the received signal moving target echoes are *contaminated* with the returns from the clutter and the electronic noise. Thus, the received signal $S(k_u, k)$ can be written, in the Fourier domain, as

$$S(k_u, k) = S_m(k_u, k) + S_0(k_u, k), \tag{10}$$

where S_0 is the term due to the clutter plus the electronic noise. To reduce the effect of S_0 we propose a digital spotlight operation applied in the spatial domain as suggested in [13]. Based on the analysis made in the previous subsection we present the following methodology to unambiguously compute μ:
1) Estimate a rough location of the moving targets using one of the strategies proposed in recent bibliography (see, e.g.,
[1], [5], or [14]).
2) Process the SAR raw-data as if there were only static targets. The ground appears focused and the

moving targets appear smeared, defocused and misplaced.

3) For each detected moving target:

3.1) Digitally spotlight the moving target image in the spatial domain and re-synthesize its signature back to the (k_u, k) domain as described in [1], obtaining the signal $\hat{S}_m(k_u, k) = S_m(k_u, k) + S_{0R}(k_u, k)$, where S_{0R} denotes the remaining noise after the digital spotlight operation (examples of spotlight regions are given in Fig. 8 in the Results section).

3.2) Compensate phase ϕ using the target approximate slant-range coordinate X', and approximate velocity magnitude $\alpha' = 1$. This is accomplished via multiplying $\hat{S}_m(k_u, k)$ by $\exp\{j\sqrt{4k^2 - (k_u/\alpha')^2}X'\}$. If a more accurate phase compensation is needed, α can be estimated using the algorithm suggested in [13].

3.3) Compute the correlation $R_{\hat{S}\hat{S}}$ between $\hat{S}_m(k_u, k_0)$ and $\hat{S}_m(k_u, k)$ for a set of discrete wavenumbers within the transmitted pulse bandwidth. We obtain then

$$\begin{aligned} R_{\hat{S}\hat{S}}(\Delta k_u, k_0, k) &= R_{SS}(\Delta k_u, k_0, k) + R_{NN}(\Delta k_u, k_0, k) \\ &\quad + R_{SN}(\Delta k_u, k_0, k) + R_{NS}(\Delta k_u, k_0, k). \end{aligned} \tag{11}$$

Terms R_{SS} and R_{NN} denote the moving target and clutter-plus-noise autocorrelations, respectively. Terms R_{NS} and R_{SN} denote the crosscorrelations. The last three terms are expected to have insignificant values when compared to R_{SS}. As shown in (7), R_{SS} shall display a maximum for each k at $\Delta k_u = 2(k - k_0)\mu$. In order to have independent clutter samples the sampling interval in the Fourier domain should be large enough (see expressions (21) and (22) in Appendix I).

3.4) Perform a linear regression on the ordinates corresponding to the maximum values of R_{SS} to estimate μ and subsequently compute the target slant-range velocity.

Notice that the suggested scheme does not require the knowledge of the parameters Y, α, or $A(k_u, k)$. It just needs an approximate value of X to estimate μ. To estimate the cross-range component of each moving target, we suggest the combination of the scheme herein proposed to estimate μ with the methodology presented by Soumekh in [1] to estimate $\alpha = \sqrt{\mu^2 + \nu^2}$. With the two quantities μ and α at hand, the estimation of ν is straightforward.

TABLE I

MISSION PARAMETERS USED IN SIMULATION.

Parameter	Value
Carrier frequency	9 GHz
Chirp bandwidth	250MHz
Altitude	12Km
Velocity	637Km/h
Look angle	20^0
Antenna radiation pattern	Raised Cosine
Oversampling factor	2

III. Estimation Results

The scheme proposed in the previous section is now applied to synthetic data and real data from the MSTAR data public collection [15]. The synthetic data set contains seven moving targets, all with cross-range velocities several times above the Nyquist limit. The experiments with MSTAR data include clutter from Hunstville-Alabama and two BTR-60 transport vehicles with simulated movement.

A. Synthetic Data

The synthetic data set includes six point-like targets and an extended target with dimensions of 6 meters in slant-range by 2 meters in cross-range. The extended target is simulated by using twelve point-like targets, all with the same reflectivity. The signal-to-clutter ratio (SCR) is set to 23dB. The mission parameters are presented in Table I. The moving targets trajectory parameters are summarized in Table II. Targets numerated from one to six are point-like targets, whereas target number seven is the extended moving target. The last column of this Table displays the ratio between the moving target slant-range velocity magnitude $|v_x|$ and the maximum slant-range velocity allowed by the mission PRF, v_{max}. Notice that all the moving targets have slant-range velocities several times larger than the Nyquist velocity. Figure 2 shows the moving targets positions and their respective velocities. Each velocity vector is represented by an arrow with length proportional to the velocity magnitude.

Figure 3 presents the target area image focused using the wavefront reconstruction algorithm [1] with static ground parameters. As expected, all the moving targets appear misplaced and blurred. To detect the moving targets we first apply high-pass filtering in the (k_u, k) domain with stop-band adjusted to filter out static targets and then perform imaging using static ground parameters. The resulting moving target indication (MTI) function is presented in Fig. 4, where we can see that all moving targets are detectable. This is a very simple scheme to detect moving targets, similar to that

TABLE II

MOVING TARGETS PARAMETERS.

Target	x_0 [m]	y_0 [m]	v_x [km/h]	v_y [km/h]	$\frac{\lvert v_x \rvert}{v_{max}}$
1	-64	-64	-13.2	-36	2.5
2	0	-64	-26.5	-36	5
3	64	-64	-52.9	-36	10
4	-64	+64	13.2	36	2.5
5	0	+64	26.5	36	5
6	64	+64	52.9	36	10
7	0	0	52.9	0	10

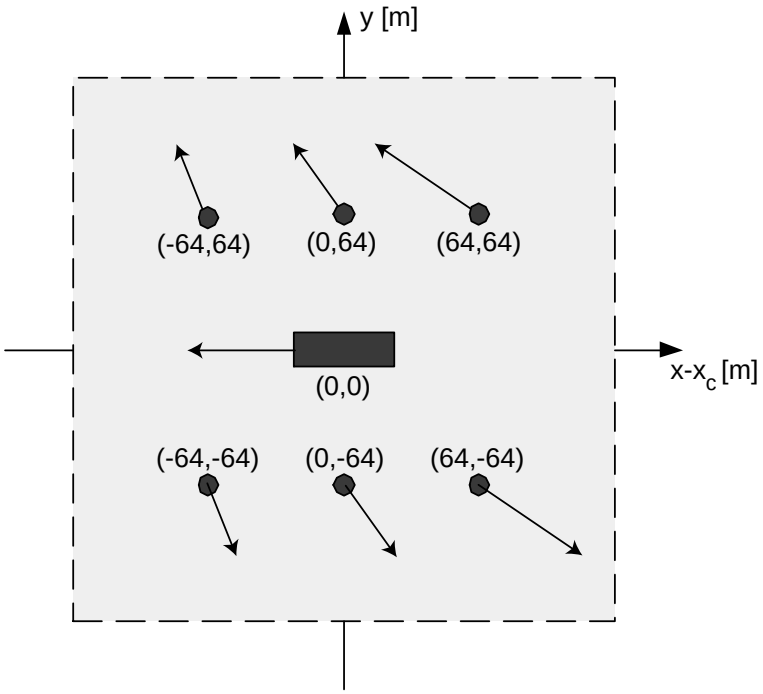

Fig. 2. Simulated positions and velocities of moving targets. The slant-range coordinates are recentered at the central slant-range coordinate x_c. The velocity vector of each target is represented by an arrow with length proportional to the velocity magnitude.

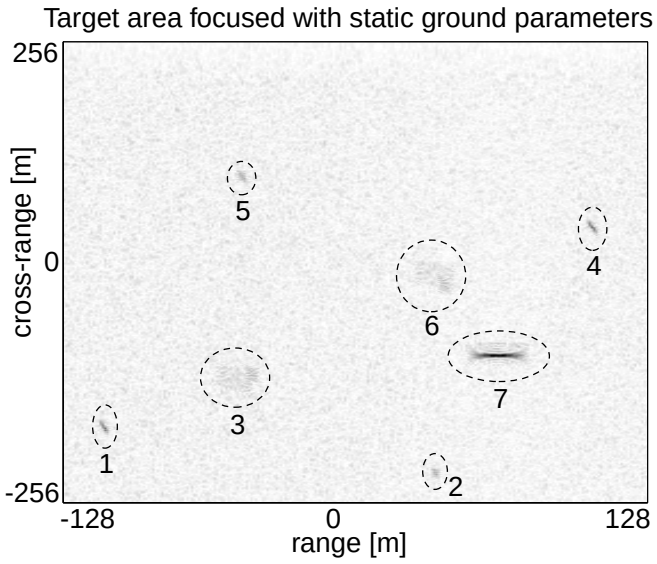

Fig. 3. Reconstructed SAR image with static ground parameters. Moving targets appear defocused and misplaced.

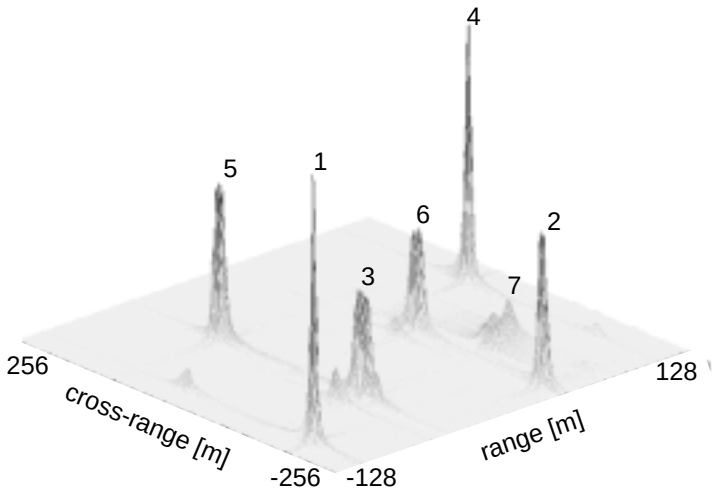

Fig. 4. Moving target indication (MTI) function after static ground filtering.

proposed by Freeman in [5]. The proposed MTI, in spite of being very simple, yields good results even for moving targets with slant-range velocities multiple of the Nyquist velocity, as far as the respective two-dimensional spectrum exhibits a non-negligible skew. In low SCR and low skew scenarios the moving target detection demands more sophisticated algorithms such as those proposed in [11], [12] [13], or [16], at expense of higher computational complexity.

For illustration purposes, we show in Fig. 5a) and Fig. 6a) the magnitude of the digitally spotlighted signatures of point-like target 3 and extended target 7, respectively.

In Fig. 5b) and Fig. 6b) we show the resulting data after performing the proposed correlation. A straight line results clearly visible in the two cases, although in the case of the moving target 7 the interaction between the multiple scatterers that compose the object causes the amplitude to fluctuate.

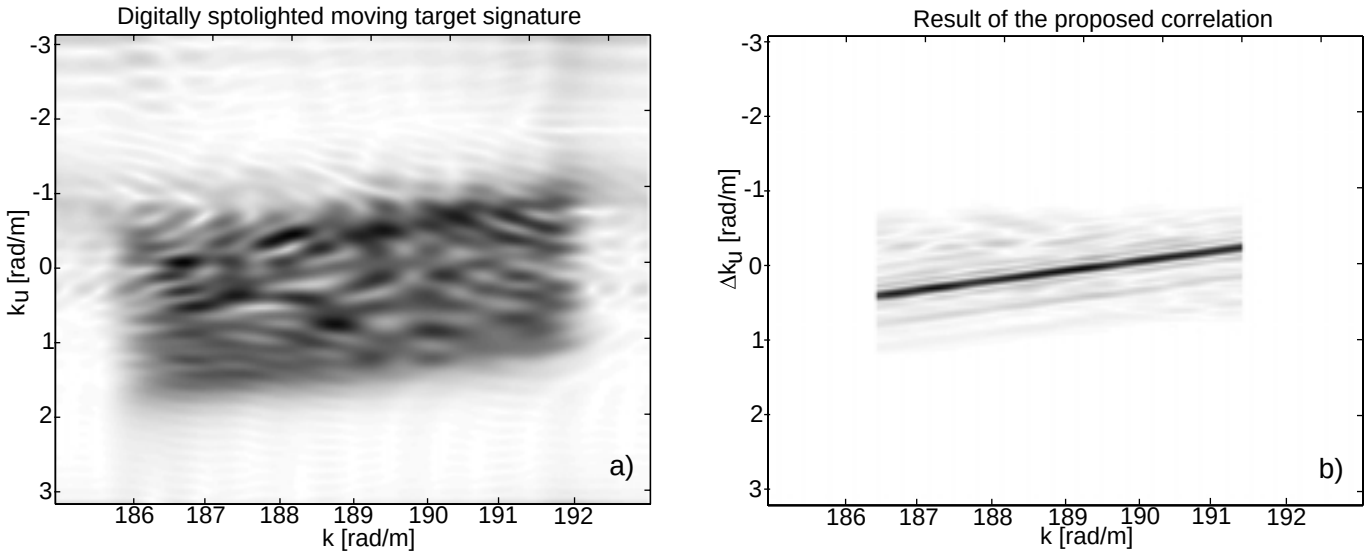

Fig. 5. a) Moving target 3 signature in the (k_u, k) domain after the digital spotlight operation. b) The maximum of the proposed correlation changes linearly with the fast-time frequency as predicted.

TABLE III

SLANT-RANGE VELOCITY ESTIMATION RESULTS (SCR=$23dB$).

Target	$v_x[km/h]$	$\hat{v}_x[km/h]$	error
1	-13.2	-13.25	0.4%
2	-26.5	-26.69	0.6%
3	-52.9	-53.21	0.6%
4	13.2	13.24	0.3%
5	26.5	26.26	0.9%
6	52.9	52.5	0.7%
7	52.9	53.03	0.3%

The slope of the resulting lines is estimated by means of a linear regression. Table III presents the slant-range velocity estimates for all the moving objects in the scene. All the estimated velocities have better accuracy than 1%, and can be used to retrieve the true Doppler interval where the moving target signature belongs.

To estimate the full velocity vector we combined the unaliased estimates of the slant-range velocity herein obtained with the estimates of the relative speed α measured as proposed by Soumekh in [1]. Table IV presents the resulting full velocity vector estimates, illustrating the usefulness of this method. With respect to the estimation of the velocity vector norm, the accuracy is better than 2%.

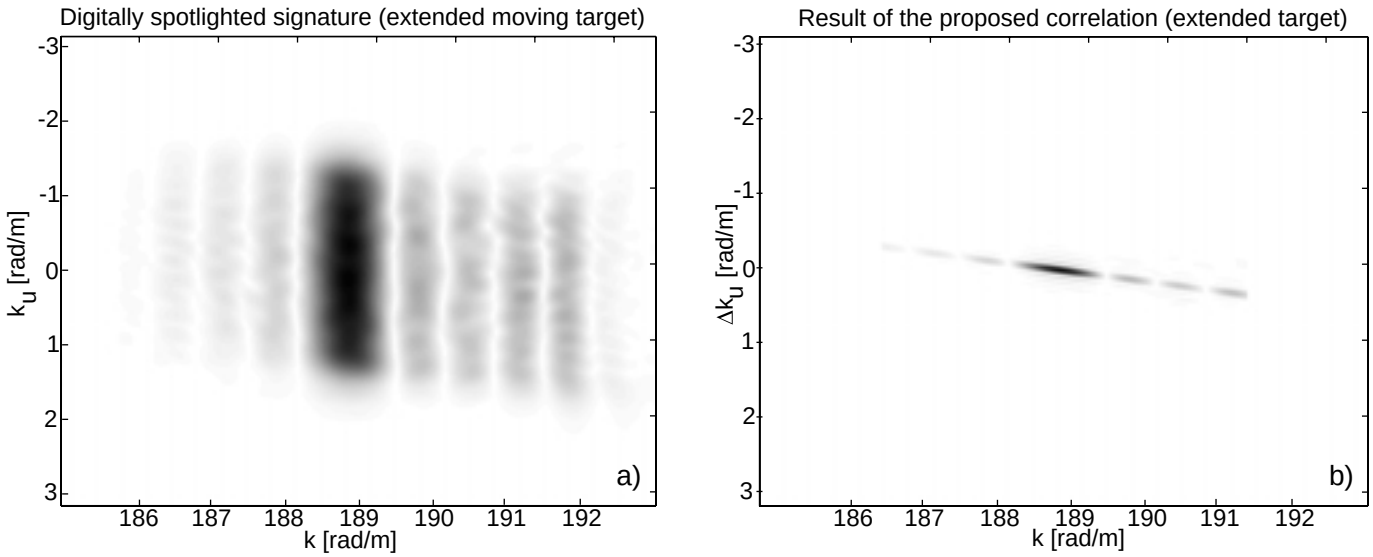

Fig. 6. a) Extended moving target 7 signature in the (k_u, k). domain after the digital spotlight operation. Bottom: Result from the proposed correlation. The maximum exhibits a fluctuation due to the interaction between the multiple scatterers that compose the object.

TABLE IV

COMPLETE VELOCITY VECTOR ESTIMATION BY JOINING TWO METHODOLOGIES (SCR=$23dB$).

Target	$(v_x, v_y)[km/h]$	$(\hat{v}_x, \hat{v}_y)[km/h]$
1	(-13.2,-36)	(-13.25,-35.53)
2	(-26.5,-36)	(-26.69,-35.78)
3	(-52.9,-36)	(-53.21,-32.9)
4	(13.2,36)	(13.24,32)
5	(26.5,36)	(26.26,38.8)
6	(52.9,36)	(52.5,37.33)
7	(52.9,0)	(53.03,1.54)

B. Real Data

In this subsection we apply the proposed strategy to real data from the MSTAR public collection. The clutter scene is taken from Huntsville, Alabama. The moving objects are two BTR-60 transport vehicles with simulated movement. The optical and X-band images of this type of vehicle are presented in Fig. 7. The mission parameters for the MSTAR data are presented in Table V.

Table VI details the moving targets velocities and coordinates. The SCR is roughly set to 23 dB. Notice that the slant-range velocities of both targets induce Doppler-shifts corresponding to 6 and 12 times the maximum unambiguous value imposed by the used PRF. The resulting data was focused using the wavefront reconstruction algorithm with static ground parameters. The obtained image is

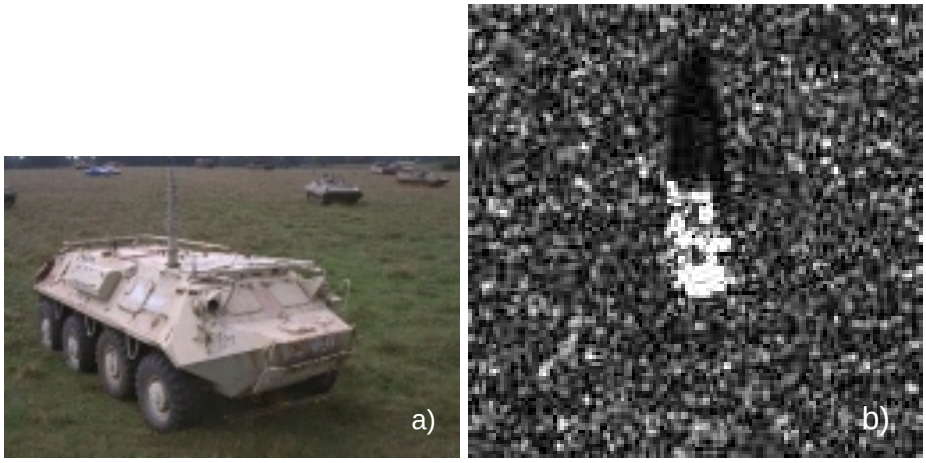

Fig. 7. BTR-60 Transport vehicle a) optical; b) X-band.

TABLE V

MISSION PARAMETERS USED WITH REAL DATA FROM MSTAR.

Parameter	Value
Carrier frequency	9.6 GHz
Chirp bandwidth	250MHz
Altitude	12Km
Velocity	637Km/h
Look angle	15^0
Antenna radiation pattern	Raised Cosine
Oversampling factor	2

TABLE VI

BTR-60 TRANSPORT VEHICLE TRAJECTORY PARAMETERS.

Target	x_0 [m]	y_0 [m]	v_x [km/h]	v_y [km/h]	$\frac{\lvert v_x \rvert}{v_{max}}$
1	75	220	29.85	36	6
2	180	122	59.69	7.2	12

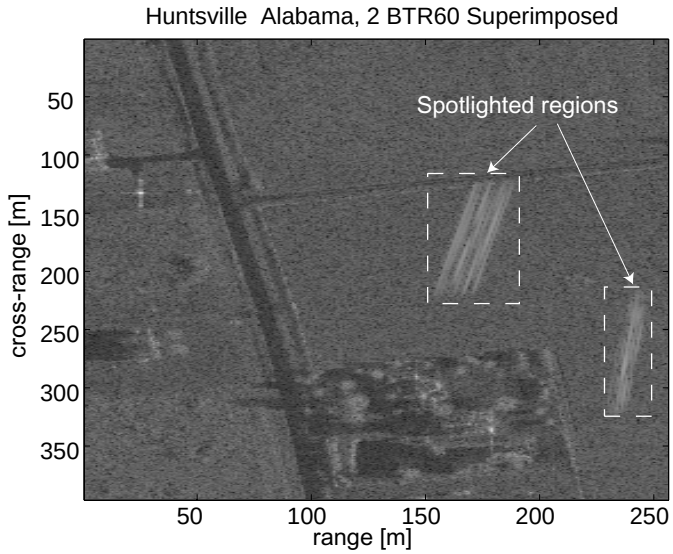

Fig. 8. Scene from Hunstville - Alabama, where two moving BTR-60 transport vehicles are superimposed. The slant-range velocity of the vehicle on the left exceeds the Nyquist limit by 6 times, whereas the vehicle on the right exceeds that velocity by 12 times. They appear defocused and misplaced as expected.

TABLE VII

SLANT-RANGE VELOCITY ESTIMATION RESULTS (SCR=$23dB$).

Target	$v_x[km/h]$	$\hat{v}_x[km/h]$	error
1	29.85	29.05	2.7%
2	59.69	61.24	2.6%

presented in Fig. 8, where the moving objects appear defocused and misplaced as expected.

Each moving object signature was digitally spotlighted in the spatial domain and resynthesized back to the (k_u, k) frequency domain as proposed in [13]. The resulting resynthesized signature in the (k_u, k) domain is presented in Fig. 9 for illustration purposes only.

The maxima of correlation (7) is shown in Fig. 10b). It varies linearly with the fast-time frequency as predicted, although exhibiting local correlation due to the interaction between the large number of scatterers that compose the BTR-60 vehicle. Nevertheless, the resulting velocity estimates are still very accurate (see Table VII).

As we did in the previous subsection, we used both estimates of μ and α to retrieve the full velocity vector. Table VIII shows the obtained results. The accuracy with respect to the estimation of the velocity vector norm is better than 4%.

C. Monte Carlo results

Figure 11 plots the standard deviation of the relative slant-range velocity by Monte-Carlo estimation (64 runs) versus the Cramer-Rao lower bound (CRLB) normalized to the number of independent

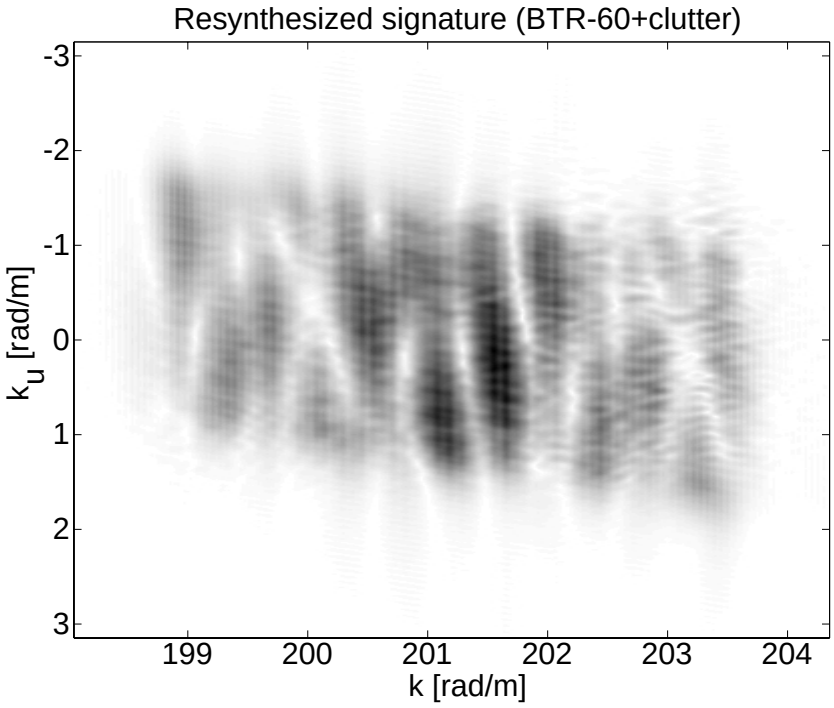

Fig. 9. Resynthesized signature of the BTR-60 plus clutter.

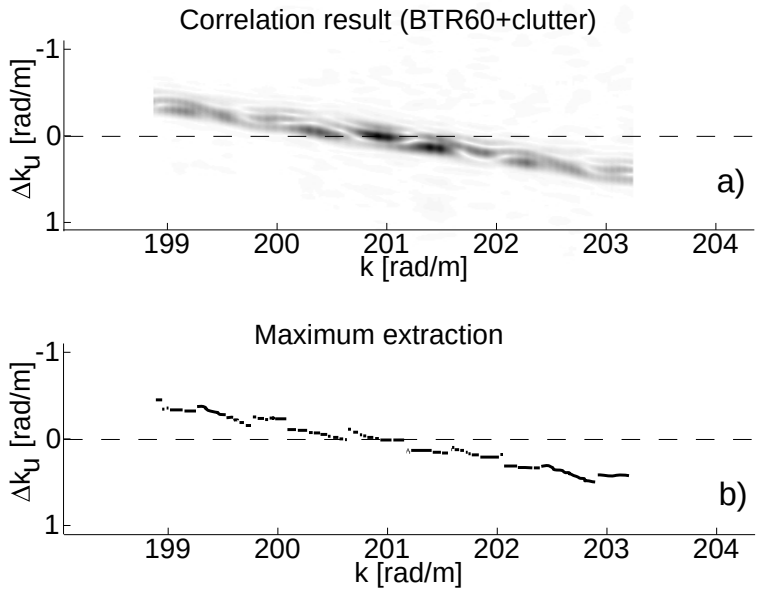

Fig. 10. a) Result of the proposed correlation for the BTR-60 vehicle moving with slant-range velocity of 12 times the maximum imposed by the mission PRF; b) Ordinates where the maximum values of the previous correlation occur. The true slant-range velocity is retrieved with an error of 2.6%.

TABLE VIII

COMPLETE VELOCITY VECTOR ESTIMATION RESULTS USING AN ASSOCIATION OF METHODOLOGIES (SCR=23dB).

Target	$(v_x, v_y)[km/h]$	$(\hat{v}_x, \hat{v}_y)[km/h]$
1	(29.85,36)	(29.05,38.91)
2	(59.69,7.2)	(61.24,8.21)

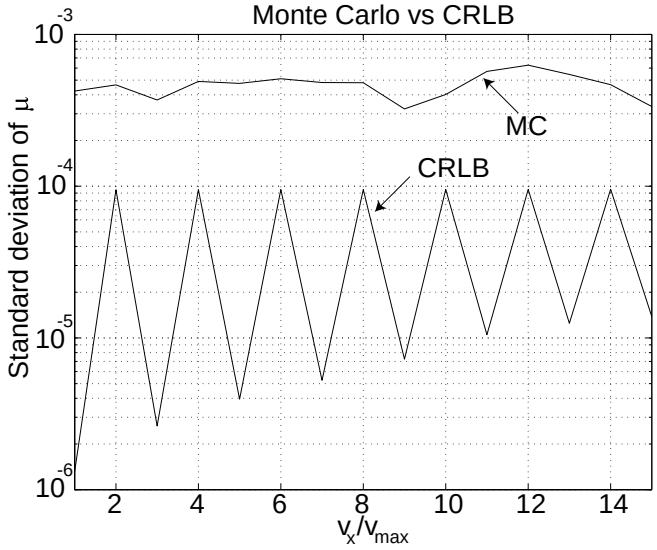

Fig. 11. Monte Carlo results (64 runs) versus Cramer-Rao Bound.

samples taken in the frequency domain (see appendix). The CRLB exhibits a periodic type pattern due to the overlapping of the moving object spectrum on the clutter spectrum when v_x/v_{max} is even. When the ratio v_x/v_{max} is odd, the overlapping is minimum and we can expect better estimation results. As it can be seen, the presented strategy performs quite well, although it does not reach the CRLB. Notice that the MC results do not present the periodic shape of the CRLB curve. This may be due to the fact that the proposed estimator, which is based on a correlation, does not include any information about the clutter statistics. If we had used the clutter covariance matrix in the derivation of the estimator we should have had the periodic behaviour present on the CRLB curve and a smaller offset between the CRLB curve and the MC results.

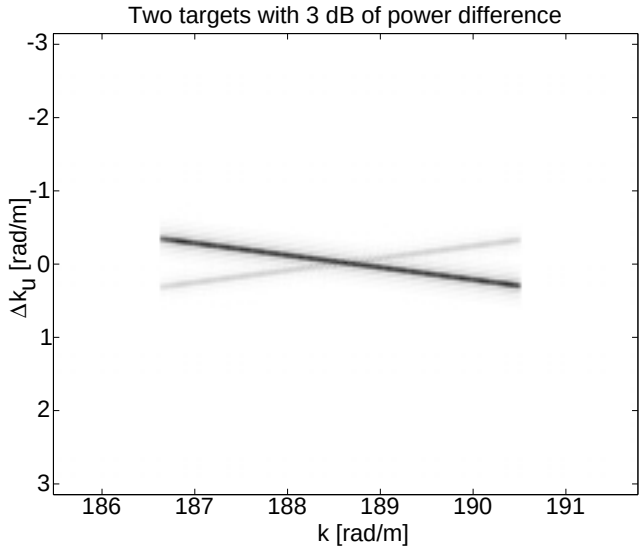

Fig. 12. Result of the proposed correlation in a scenario where two moving objects with different reflectivities and opposite slant-range speeds are present. As expected, the result are two lines with distinct intensities and opposing slopes.

D. Violation of assumptions

The proposed methodology to obtain the slant-range velocity of the moving objects relies on the following assumptions:

i) Targets are separable from each other in the spatial domain;

ii) The clutter that remains after the digital spotlight operation shows small correlation in the frequency domain.

In this subsection we will illustrate the result of the proposed correlation when the previous assumptions are violated.

We start with a scenario containing two moving objects with slant-range velocities 10 times greater than v_{max}, but traveling in opposite directions. Both targets were simulated to appear overlapped in the unfocused image. One of the objects has reflectivity 3 dB greater than the other. In this case the digital spotlight operation cannot isolate one object from the other. Both signatures will thus be used simultaneously in the computation of the correlation (7). Correlation result is shown in Fig. 12, where two lines with different intensities and symmetric slopes are clearly distinguishable, each one corresponding to a moving target. The two distinct intensities are due to the different reflectivities of the moving objects.

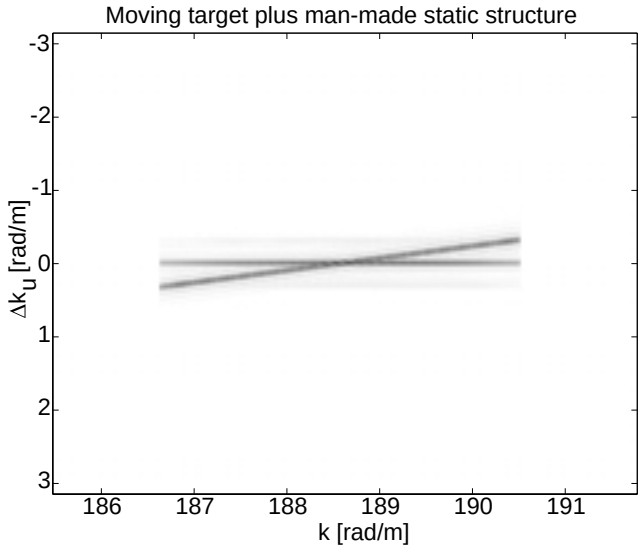

Fig. 13. Result of the proposed correlation in a scenario where the digital spotlight operation is not able to separate the moving vehicle from a man made static structure. The resulting horizontal line is due to the static structure. The off-horizontal line is due to the moving object.

In the next example we violate the assumption that the clutter exhibits small correlation. To accomplish this purpose we simulated a moving object that appears superimposed on a man-made structure after focusing with static ground parameters. The used man-made structure is the one positioned at coordinates (cross-range, slant-range)=(131,39) in Fig. 8. The digital spotlight operation is not able to separate the two objects. Correlation maxima is presented in Fig. 13, where two lines with different slopes are clearly visible. The horizontal line is due to the static man-made structure. The line with non-zero slope is originated by the moving target.

In the previous examples we saw that we cannot simply apply the last step of the proposed algorithm, which consists on a linear regression on the correlation maxima. A more sophisticated scheme is thus necessary. We will address these scenarios in the near future.

IV. Conclusions and Final Remarks

In this paper we have presented a novel methodology to retrieve unaliased estimates of the slant-range velocity of moving targets inducing Doppler-shifts beyond the Nyquist limit imposed by the mission PRF. We exploited the linear dependency of the Doppler-shift with the slant-range velocity for each fast-time frequency. That is, the echo from a moving object, in the two-dimensional frequency domain, exhibits a skew not subject to PRF limitations. We proposed an estimator of the spectrum skew and have illustrated its usefulness using a combination of real and synthetic data. The accuracy was shown to depend on the emitted pulse bandwidth. Basically, this is due to the fact that by using larger bandwidth we have more independent samples to feed the estimator and therefore we have lower variance on the resulting velocity estimates. The method was shown to give good results even when the returned echo overlaps completely those echoes from the static ground, provided that the moving targets signatures are digitally spotlighted.

By combining the methodology proposed herein with an existing methodology to retrieve the velocity vector magnitude we have shown that it is possible to estimate the full velocity vector with good accuracy using aliased data from a single SAR sensor.

The major limitations of the proposed approach are the following assumptions: i) moving target reflectivity is independent of the aspect angle; ii) moving target is point-like target or it contains predominant scatterers, thus exhibiting near point-like behaviour. The former assumption greatly simplifies the problem formulation and yet leads to good-results. The later assumption is reasonable as most man-made targets can be considered to be a set of individual point-like scatterers [17].

Appendix

I. Ground Returns Covariance in the slow-time and fast-time frequency domain

In this section we show that the covariance of the echoes returned from the static ground in the slow-time and fast-time frequency domains decays very quickly if we consider the clutter to be homogeneous with a large number of scatterers per resolution cell.

The returned echo from the static ground can be written as [1], [11], [18]

$$S(k_u,\omega) = |P(\omega)|^2 A(k_u,\theta_0)\sum_n f_n e^{-\xi_n(k_u,\omega)}, \tag{12}$$

where f_n is the reflectivity of the nth static scatterer with coordinates (x_n, y_n), symbol $\theta_0 \equiv (\mu_0,\nu_0) = (0,1)$, and

$$\xi_n(k_u,\omega) \equiv \sqrt{4k^2 - k_u^2}x_n + k_u y_n. \tag{13}$$

The covariance of S

$$C_S(k_{u_1},k_{u_2},\omega_1,\omega_2) \equiv E\left[S(k_{u_1},\omega_1)S^*(k_{u_2},\omega_2)\right], \tag{14}$$

is therefore

$$\begin{aligned} &C_S(k_{u_1},k_{u_2},\omega_1,\omega_2) = \\ &= E\Big[|P(\omega_1)|^2|P(\omega_2)|^2 A(k_{u_1},\theta_0)A^*(k_{u_2},\theta_0) \\ &\times \sum_n f_n e^{-j\xi_n(k_{u_1},\omega_1)}\sum_m f_m^* e^{j\xi_m(k_{u_2},\omega_2)}\Big]. \end{aligned} \tag{15}$$

If the number of scatterers per resolution cell is large, none is predominant, they are mutually independent, and each one has phase independent of its amplitude then $E[f_n f_m^*] = 0$ if $n \neq m$ and $E[f_n f_m^*] \equiv \sigma_n$ if $n = m$. The covariance is therefore written as

$$\begin{aligned} &C_S(k_{u_1},k_{u_2},\omega_1,\omega_2) = \\ &= \underbrace{|P(\omega_1)^2||P(\omega_2)^2|A(k_{u_1},\theta_0)A^*(k_{u_2},\theta_0)}_{\Gamma(k_{u_1},k_{u_2},\omega_1,\omega_2)} \\ &\times \sum_n \sigma_n e^{-j\left[\xi_n(k_{u_1},\omega_1)-\xi_n(k_{u_2},\omega_2)\right]}. \end{aligned} \tag{16}$$

Using the approximation, $\sqrt{4k^2-k_u^2} \approx 2k - \frac{k_y^2}{4k}$, valid for $k \gg k_u$, we get

$$\begin{aligned} &C_S(k_{u_1},k_{u_2},\omega_1,\omega_2) \approx \Gamma(k_{u_1},k_{u_2},\omega_1,\omega_2) \\ &\times\sum_n \sigma_n e^{-2j(k_1-k_2-\frac{k_{u_1}^2}{4k_1}+\frac{k_{u_2}^2}{4k_2})x_n} e^{-j(k_{u_1}-k_{u_2})y_n}. \end{aligned} \tag{17}$$

Let us consider an homogeneous scene with constant backscattering coefficient given by

$$\sigma_0 = \frac{1}{\Delta}\sum_{n:(X_n,Y_n)\epsilon\Delta(X',Y')}\sigma_n, \tag{18}$$

where $\Delta(X', Y')$ is a small rectangle of area Δ centered at (X', Y'). Expression (17) can thus be approximated by

$$C_S(k_{u_1}, k_{u_2}, \omega_1, \omega_2) \approx \Gamma(\omega_1, \omega_2, k_{u_1}, k_{u_2})\sigma_0 \times \int_{-L_x/2}^{L_x/2} \int_{-L_y/2}^{L_y/2} e^{-j2(k_1 - \frac{k_{u_1}^2}{4k_1} - k_2 + \frac{k_{u_2}^2}{4k_2})x} e^{j(k_{u_1} - k_{u_2})y} dxdy, \tag{19}$$

where L_x and L_y are the target area lengths in slant-range and cross-range directions, respectively. After some algebraic manipulation we are lead to

$$\begin{aligned} C_S(k_{u_1}, k_{u_2}, \omega_1, \omega_2) \approx \Gamma(k_{u_1}, k_{u_2}, \omega_1, \omega_2)\sigma_0 L_x L_y \\ \times \quad \text{sinc}\left[\frac{k_{u_1} - k_{u_2}}{2\pi} L_y\right] \\ \times \quad \text{sinc}\left[\frac{\left((k_1 - \frac{k_{u_1}^2}{4k_1}) - (k_2 - \frac{k_{u_2}^2}{4k_2})\right)}{\pi} L_x\right]. \end{aligned} \tag{20}$$

Longer L_x and L_y lead to more localized main-lobes of the sinc functions. In the slow-time frequency axis the covariance C_s is null for

$$|k_{u_1} - k_{u_2}| = \frac{2\pi}{L_y}, \tag{21}$$

and in the fast-time frequency axis the covariance is zero for

$$|k_1 - k_2| = \frac{\pi}{L_x}. \tag{22}$$

If take samples in the frequency domain with spacing given by (21) and (22) then those samples will also be independent.

II. Theoretical bounds

In this section we compute the Cramer-Rao lower bound (CRLB) for the velocity components of moving targets.

As we saw previously, the returned echo from the static ground, after pulse compression is

$$S_0(k_u,\omega) = |P(\omega)|^2 A(k_u,\theta_0)\sum_n f_n e^{-\xi_n(k_u,\omega)}, \tag{23}$$

where

$$\xi_n(k_u,\omega) = \sqrt{4k^2 - k_u^2}x_n + k_u y_n, \tag{24}$$

and $\theta_0 = (\mu_0,\nu_0) = (0,1)$ denotes the velocity vector parameters for the static ground. For a point-like moving target with motion transformed coordinates (X,Y) and complex reflectivity f_m, the echoed signal is [1], [11]

$$S_m(k_u,\omega) = |P(\omega)|^2 A(k_u,\theta) f_m e^{-\xi_m(k_u,\omega,\alpha)}, \tag{25}$$

where, $\alpha = \sqrt{\mu^2+\nu^2}$ and $\theta = (\mu,\nu)$ and

$$\xi_m(k_u,\omega,\alpha) = \sqrt{4k^2 - (k_u/\alpha)^2}X + (k_u/\alpha)Y. \tag{26}$$

The total echo returned due to the static ground and the moving target is thus

$$S(k_u,\omega) = S_0(k_u,\omega) + S_m(k_u,\omega). \tag{27}$$

Let us define the vector

$$\boldsymbol{S} \equiv [S_{-N}\cdots S_0 \cdots S_N]^T, \tag{28}$$

for a fixed fast-time frequency ω_c, where, $S_i \equiv S(k_{u_i},\omega_c)$, $k_{u_i} = \frac{i}{2N}\Delta K$ for $i = -N,\cdots,N$, and symbol ΔK denotes the spatial sampling frequency. In order to have independent samples, the sampling frequency ΔK is selected according to eq. (22). Define also $\boldsymbol{A}(\theta) \equiv [A_{-N}(\theta)\cdots\ A_0(\theta)\cdots A_N(\theta)]^T$, where $A_i(\theta) \equiv A(k_{u_i},\theta)$.

Let us assume that the number of static scatterers per resolution cell is large, none is predominant, the echo amplitudes f_n are mutually independent and have phase uniformly distributed in a 2π interval. Therefore, the vector $\boldsymbol{S}$ is complex circular zero-mean and Gaussian. The density of vector $\boldsymbol{S}$ conditioned to θ and the target reflectivity can thus be written as

$$p(\boldsymbol{S}|f_m,\theta) = \frac{1}{2\pi^N|\boldsymbol{C}_s|}e^{-(\boldsymbol{S}-\boldsymbol{m}_s)^H\boldsymbol{C}_s^{-1}(\boldsymbol{S}-\boldsymbol{m}_s)}, \tag{29}$$

where the mean $\boldsymbol{m}_s$ is given by

$$\boldsymbol{m}_s = f_m|P(\omega_c)|^2\boldsymbol{A}(\theta)\boldsymbol{\xi}, \tag{30}$$

and $\boldsymbol{\xi} = \mathrm{diag}(\xi_i)$ and $\xi_i = \xi_m(k_{u_i},\omega_c,\alpha)$.

As already shown in the previous appendix, the inverse of the covariance matrix $\boldsymbol{C}_s$ is given by

$$\boldsymbol{C}_s^{-1} = \frac{1}{|P(\omega_c)|^4 P L_x L_y} \mathrm{diag}(|A(k_{ui}, \theta_0)|^{-2}). \tag{31}$$

The elements of the Fisher information matrix for a circular complex Gaussian process are given by [19]

$$\begin{aligned} [I(\boldsymbol{\theta})]_{ij} &= tr\left[\boldsymbol{C}_s^{-1}(\boldsymbol{\theta}) \frac{\delta \boldsymbol{C}_s(\boldsymbol{\theta})}{\delta \theta_i} \boldsymbol{C}_s^{-1}(\boldsymbol{\theta}) \frac{\delta \boldsymbol{C}_s(\boldsymbol{\theta})}{\delta \theta_j}\right] \\ &+ 2Re\left[\frac{\delta \boldsymbol{m}_s{}^H(\boldsymbol{\theta})}{\delta \theta_i} C_s^{-1}(\boldsymbol{\theta}) \frac{\delta \boldsymbol{m}_s(\boldsymbol{\theta})}{\delta \theta_j}\right], \\ & i, j = 1, 2. \end{aligned} \tag{32}$$

The first term in equation (32) is null because the noise covariance matrix is independent of the moving target parameters. After some lengthy algebraic manipulation we achieve the following expressions for the Fisher matrix elements:

$$\begin{aligned} I_{11}(\theta) = \frac{2|f_m|^2}{P L_x L y} &\left[\sum_i \frac{|A_i(\theta)|^2}{|A_i(\theta_0)|^2} k_{ui}^2 \mu^2 \right. \\ \times &\left. \left(\frac{k_{ui} X}{\alpha^2 \sqrt{4k^2 - (k_{ui}/\alpha)^2}} - \frac{Y}{\alpha^3}\right)^2 + \frac{k^2}{\nu^2} \sum_i \frac{|\dot{A}_i(\theta)|^2}{|A_i(\theta_0)|^2}\right] \end{aligned} \tag{33}$$

$$\begin{aligned} I_{12}(\theta) &= I_{21}(\theta) = \frac{|f_m|^2}{P L_x L y} \left[2\mu\nu \sum_i \frac{|A_i(\theta)|^2}{|A_i(\theta_0)|^2} k_{ui}^2 \right. \\ &\times \left. \left(\frac{k_{ui} X}{\alpha^2 \sqrt{4k^2 - (k_{ui}/\alpha)^2}} - \frac{Y}{\alpha^3}\right)^2 \right. \\ &+ \left. \frac{k}{\nu^3} \sum_i (k_{ui} - 2k\mu) \frac{|\dot{A}_i(\theta)|^2}{|A_i(\theta_0)|^2}\right] \end{aligned} \tag{34}$$

$$\begin{aligned} I_{22}(\theta) &= \frac{|f_m|^2}{2 P L_x L y} \left[4\nu^2 \sum_i \frac{|A_i(\theta)|^2}{|A_i(\theta_0)|^2} k_{ui}^2 \right. \\ &\times \left. \left(\frac{k_{ui} X}{\alpha^2 \sqrt{4k^2 - (k_{ui}/\alpha)^2}} - \frac{Y}{\alpha^3}\right)^2 \right. \\ &+ \left. \frac{(k_{ui} - 2k\mu)^2}{\nu^4} \sum_i (k_{ui} - 2k\mu) \frac{|\dot{A}_i(\theta)|^2}{|A_i(\theta_0)|^2}\right]. \end{aligned} \tag{35}$$

The Cramer-Rao Bound for μ and ν are given by the inverse of the Fisher Information matrix (principal diagonal elements), that is, $\mathrm{CRLB}(\mu) = [I^{-1}(\theta)]_{11}$ and $\mathrm{CRLB}(\nu) = [I^{-1}(\theta)]_{22}$.

The estimation technique proposed in this paper uses several measurements in the available pulse bandwidth. Therefore, the variance of the achieved estimates must be compared with the values of the CRLB after the linear regression.

Let us consider that each measurement has variance $[I^{-1}(\theta)]_{11}$ (we ignore quantization errors). If the number of independent measurements is N, and the spacing between each measurement in the fast-time frequency is Δ_k, then the variance after the linear regression is

$$\sigma_\mu^2 = \frac{3\text{CRLB}(\mu)}{\Delta_k^2 N(N+1)(N+2)}. \tag{36}$$

This result states that the accuracy of the slant-range velocity estimates shall increase by augmenting the number of independent observations and by enlarging the transmitted pulse bandwidth. In section III of the main text we plot CRLB curves and compare those with the results obtained via Monte Carlo simulations.

III. ACKNOWLEDGMENTS

The authors would like to acknowledge the Air Force Research Laboraty (AFRL) and the Defense Advanced Research Projects Agency (DARPA) for MSTAR data they promptly made available to us.

References

[1] Mehrdad Soumekh, *Synthetic Aperture Radar Signal Processing with MATLAB algorithms*, WILEY-INTERSCIENCE, 1999.

[2] R. Keith Raney, "Synthetic aperture imaging radar and moving targets", *IEEE Transactions on Aerospace and Electronic Systems*, vol. AES-7, pp. 499–505, 1971.

[3] P. Marques and J. Dias, "Optimal detection and imaging of moving objects with unknown velocity", *in Proc. of the 3rd European Conference on Synthetic Aperture Radar, EUSAR 2000*, pp. 561–564, 2000.

[4] S. Barbarossa and A. Farina, "Space-time-frequency processing of synthetic aperture radar signals", *IEEE Transactions on Aerospace and Electronic Systems*, vol. 30, pp. 341–358, April 1994.

[5] A. Freeeman and A. Currie, "Synthetic aperture radar (sar) images of moving targets", *GEC Journal of Research*, vol. 5, pp. 106–115, 1987.

[6] Genyuan Wang, Xiang-Gen Xia, Victor C. Chen, and Ralph L. Fiedler., "Detection, location and imaging of fast moving targets using multi-frequency antenna array sar (mf-sar)", *in Proc. of the 3rd European Conference on Synthetic Aperture Radar, EUSAR 2000*, pp. 557–560, 2000.

[7] S. Barbarossa, "Detection and imaging of moving objects with synthetic aperture radar", *IEE Proceedings-F*, vol. 139, pp. 79–88, February 1992.

[8] J. A. Legg, A. G. Bolton, and D. A. Gray, "Sar moving target detection using non-uniform pri", *in Proc. of the 1st European Conference on Synthetic Aperture Radar EUSAR'96*, pp. 423–426, 1996.

[9] Xiang-Gen Xia, "On estimation of multiple frequencies in undersampled complex valued waveforms", *IEEE Transactions on Signal Processing*, vol. 47, pp. 3417–3419, December 1999.

[10] R. Bamler and H. Runge, "Prf-ambiguity resolving by wavelength diversity", *IEEE Transactions on Geoscience and Remote Sensing*, vol. 29, pp. 997–1003, November 1991.

[11] J. Dias and P. Marques, "Moving targets detection and trajectory parameters estimation using a single sar sensor", *IEEE Tansactions on Aerospace and Electronic Systems*, vol. (submitted), 2002.

[12] Joachim H. G. Ender, "Detection and estimation of moving target signals by multi-channel sar", *in Proc. of the 1st European Conference on Synthetic Aperture Radar, EUSAR'96*, pp. 411–417, 1996.

[13] Mehrdad Soumekh, "Reconnaissance with ultra wideband uhf synthetic aperture radar", *IEEE Signal Processing Magazine*, vol. , pp. 21–40, July 1995.

[14] D. Blacknell, "Target detection in correlated sar clutter", *IEEE Proceedings on Radar, Sonar and Navigation*, vol. 147, pp. 9–16, February 2000.

[15] V. Velten J. Mossing T. Ross, S. Worrell and M. Bryant, "Standard sar atr evaluation experiments using the mstar public release data set", *in SPIE Proceedings: Algorithms for Synthetic Aperture Radar Imagery V*, pp. 566–573, 1998.

[16] J. R. Fienup, "Detecting moving targets in sar imagery by focusing", *IEEE Tansactions on Aerospace and Electronic Systems*, vol. 37, pp. 794–809, July 2001.

[17] V. C. Chen and Hao Ling, "Joint time-frequency analysis for radar signal and image processing", *IEEE Signal Processing Magazine*, vol. 16, pp. 81–93, March 1999.

[18] P. Marques and J. Dias, "Moving targets in synthetic aperture images: A bayesian approach", *in Proc. of the International Conference on Image Processing, ICIP 2000*, 2000.

[19] S. Kay, *Fundamentals of Statistical Signal Processing. Estimation Theory*, Prentice-Hall, Englewood Cliffs, NJ, 1993.